# Atmospheric positron flux modulation during thunderstorms

A. Chilingarian and B. Sargsyan
*A I Alikhanyan National Lab (Yerevan Physics Institute), Yerevan 0036, Armenia*

(Received 4 August 2023; accepted 12 February 2024; published 8 March 2024)

We have discovered a new phenomenon in high-energy atmospheric physics involving an increased fraction of ground-level positrons during a thunderstorm. This increase is linked to developing a lower positively charged region (LPCR) at the thundercloud bottom. When the electric field strength in the lower atmosphere exceeds a critical value, seed electrons from cosmic rays accelerate and multiply, creating relativistic runaway avalanches of millions of electrons and gamma rays with energies up to 50 MeV. The emerging LPCR changes the polarity of the electric field nearly to the Earth's surface, causing electrons to decelerate and positrons to accelerate, increasing the flux of 511 keV "annihilation" gamma rays. By measuring these gamma rays, we can reveal the formation of the LPCR and follow the dynamics of the charge structure in the lower part of the thundercloud.

DOI: 10.1103/PhysRevD.109.062003

## I. INTRODUCTION

The cosmic ray flux is affected by the electrostatic fields that emerge in the thunderous atmosphere, which are linked to charge structures in the thundercloud. The modern understanding of the typical distribution of charges in a cloud and the resulting electric field is associated with experiments on the highest peak of Germany, Zugspitze [1], in 1945–1948. The experiments performed by Joachim Küttener revealed a more complex structure of the intracloud electric field than the "classical" Wilsonian dipole [2]. The main negatively charged layer in the middle of the thundercloud and its mirror in the ground form a dipole that causes electrons to accelerate downwards toward the earth's surface. Suppose the strength of the electric field is above a certain threshold (critical value). In that case, it can trigger a relativistic runaway electron avalanche (RREA, [3]) that can reach the Earth's surface and cause a thunderstorm ground enhancement (TGE, [4,5]). This significantly increases electron, gamma ray, and neutron fluxes measured by surface particle detectors.

Küttener found a small positive charge area in the cloud's lower part (lower positive charge region; LPCR). In addition, he determined that the positive charge is concentrated on graupel, a particular aggregate state of water (water in an ice shell). Not everyone immediately grasped the significance of Küttner's discovery. In 1963, Richard Feynman wrote: "The top of the thunderstorm is positively charged and the bottom negative, except for a small local area of positive charge at the bottom of the cloud, which caused much concern for everyone. No one seems to know why he is there or how important he is. If it weren't for him, everything would be much easier" [6]. However, further investigations of cloud-charged structure [7] confirm the tripole structure of cloud charge and the role of "graupel" hydrometeors in the forming of the transient LPCR. According to modern concepts, LPCR is essential for charge separation in the cloud and lightning initiation [8,9]. In its absence, the direction of the lightning will most likely be towards the upper positive charge. Thus, without this "useless" local area of positive charge, our planet may be quiet, dark, and lifeless.

The LPCR mirrors itself in the Earth, forming a third dipole in the lowest part of the thundercloud. This dipole modulates the flux of positrons, which are being accelerated, and electrons, which are being decelerated. Thus, in a tripole structure of the atmospheric electric field (AEF), two dipoles accelerate electrons downwards, while the third dipole accelerates positrons downwards towards the Earth's surface. The LPCR is temporary and disappears with a graupel fall, which leads to fast changes in the cloud's charge structure. This, in turn, quickly modifies the AEF and the acceleration and deceleration modes of charged particles.

The development of the LPCR can be seen in the shift from negative to positive near-surface electric field (NSEF) readings captured by BOLTEK's EFM-100 sensor. This sensor is commonly used in atmospheric physics research and can measure NSEF and the distance to the lightning flashes at distances up to 33 km with a frequency of 20 Hz. The NSEF measurements are transmitted via WiFi to online computers and stored in a MySQL database. Typically, we rely on the 1-second averaged time series of the NSEF for multivariate visualization and correlation analysis. The ORTEC-905-4 model is utilized for natural gamma ray radiation (NGR) spectroscopy. This gamma spectrometer is equipped with a $3'' \times 3''$ NaI (Tl) crystal, has 1024 measuring channels, excellent stability, and a relative energy resolution of full width at half maximum 7–10% at energies of 0.3–1.5 MeV.

 

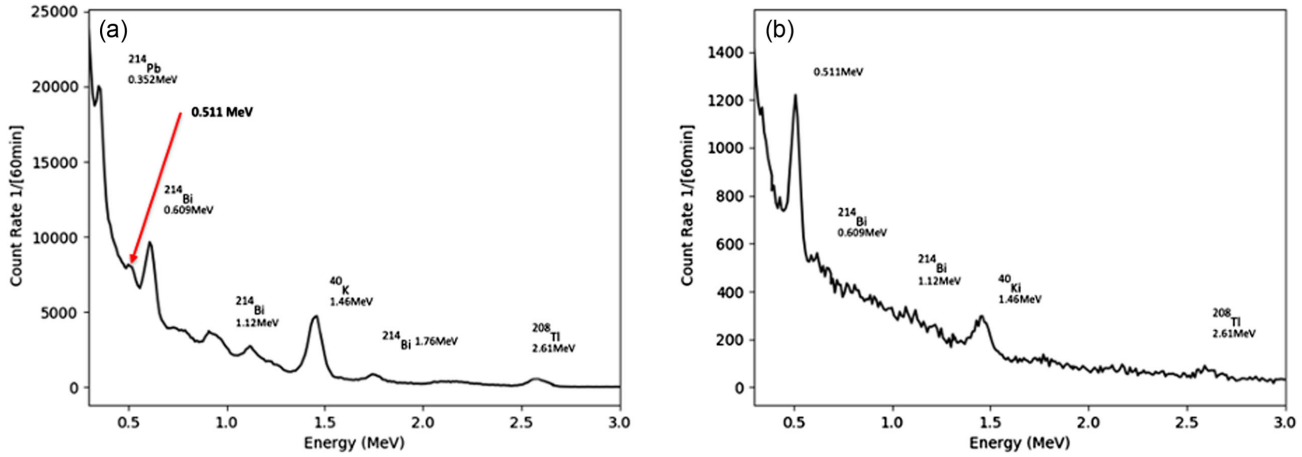


FIG. 1. NGR spectrograms obtained with the ORTEC spectrometer during an hour exposition without a lead filter (a) and with a 4 cm lead filter (b). In frame (a), the 511 keV peak is shown by the red arrow.

This paper reports an increase in the positron flux during thunderstorms and how it links to the cloud charge structure.

## II. EXPERIMENTAL ARRANGEMENT

During the spectroscopic measurement of NGR in 2019 [10], we detected an increase in the intensity of the 511 keV annihilation peak. During thunderstorms, the flux of electrons and positrons modulated by the atmospheric electric field increased compared to the fair-weather value. However, this peak had been contaminated by Compton scattered gamma rays (in the body of the NaI crystal) of higher energies from the Radon decay chain, particularly from $^{214}$Bi isotope (609 keV), see Fig. 1(a), a large peak near a small 511 keV peak. To reduce background interference, we utilized 4 cm thick lead bricks surrounding the spectrometer from the bottom and all sides, leaving only the top open. This effectively suppressed the Radon progeny gamma radiation, as shown in Fig. 1(b). As a result, the overall intensity of NGR decreased by approximately ten times. However, the 511 keV peak's relative size became much larger compared to $^{214}$Bi, Fig. 1(b).

Table I shows the numerical version of the hourly count rates of significant isotopes that make up the NGR, as presented in Fig. 1. The second row shows the energy range around the emission line of each isotope and the 511 keV line from which the isotopes were selected. The third row of the table displays the hourly count rates of the ORTEC spectrometer corresponding to Fig. 1(a), without lead bricks. The fourth row of the table shows the reduced count rates after the ORTEC spectrometer was covered with a lead filter. The last row shows the relative decrease of the count rates. According to Table I, the contamination of the $^{214}$Bi isotope decreased 47 times from 26135 to 557 counts per hour. In contrast, the 511 KeV annihilation gamma ray flux decreased only 3.5 times from 10223 to 2927 counts per hour. Despite this reduction, the 511 keV peak overwhelms the background, as shown in Fig. 1(b).

## III. ENHANCEMENT OF THE NGR DURING THUNDERSTORMS DUE TO RADON CIRCULATION EFFECT

A strong AEF initiates particle avalanches in the atmosphere above particle detectors. At the same time, the NSEF, induced by the AEF, lifts charged aerosols with attached charged radon progeny into the atmosphere (radon circulation effect [11]). The spontaneous gamma radiation of radon progeny is almost isotropic and prolonged to tens of meters and more above the ground. In turn, atmospheric positrons, coming from the near-vertical direction, annihilate with electrons above the spectrometer, and the 511 keV gamma rays enter the spectrometer mainly from the forward direction. To isolate the radiation of the lifted isotopes from the enhanced during TGEs 511 keV gamma

TABLE I. One-hour count rates of main components responsible for NGR.

| Counts per hour | Sum MeV | 0.511 MeV | 214Pb 0.352 MeV | 214Bi 0.609 MeV | 214Bi 0.768 MeV | 228AC 0.911 MeV | 214Bi 1.12 MeV | 40K 1.46 MeV | 214Bi 1.76 MeV | 214Bi 2.2 MeV | 208Tl 2.61 MeV | Cosmic ray+ Compton scattered |
|---|---|---|---|---|---|---|---|---|---|---|---|---|
| Energy range | [0.3–3] | [0.47–0.55] | [0.324–0.38] | [0.56–0.66] | [0.7–0.83] | [0.84–0.98] | [1–1.2] | [1.34–1.57] | [1.62–1.89] | [2–2.4] | [2.41–2.82] | [0.3–3] |
| Lead free | 661464 | 10223 | 26797 | 26135 | 2489 | 8940 | 7632 | 33332 | 3377 | 3348 | 5264 | 533927 |
| 4 cm lead | 67990 | 2927 | 846 | 557 | 146 | 249 | 505 | 1497 | 294 | 129 | 226 | 60614 |
| 4 cm lead/free | 9.7 | 3.5 | 32 | 47 | 17 | 36 | 15 | 22 | 11.5 | 26 | 23 | 8.8 |

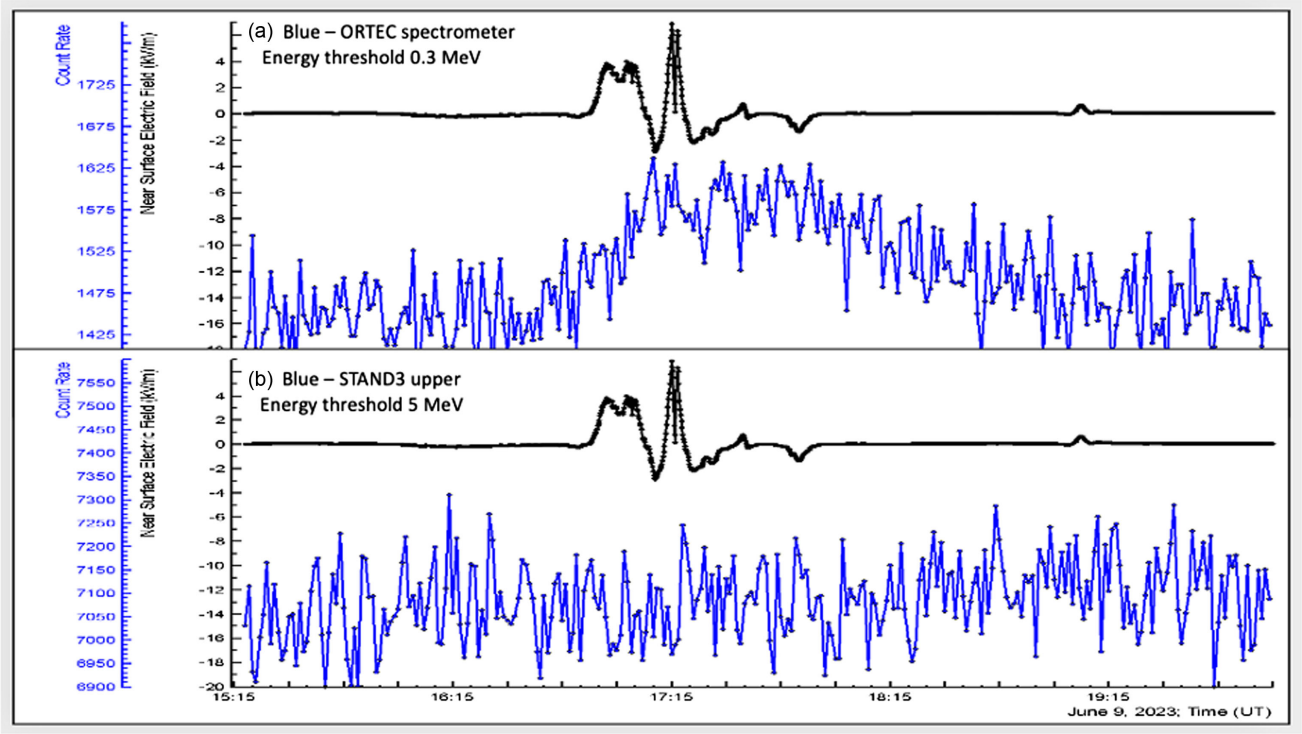


FIG. 2. (a) Disturbances of NSEF (black curve); 1-minute time series of count rates of ORTEC spectrometer, energy threshold 0.3 MeV (blue curve). (b) Disturbances of NSEF (black curve); 1-minute time series of count rates of STAND3 upper scintillator, energy threshold: 5 MeV (blue curve). The atmospheric electric field does not initiate RREA; induced NSEF causes enhancement of NGR.

ray flux, we selected events when the strength of the AEF was not strong enough to initiate particle avalanches (RREAs). The radon circulation is not a threshold process as RREA is, and it enhanced the NGR at almost all NSEF values above a few kV/m. In Fig. 2, we demonstrate the selection procedure. In Fig. 2(a), along with disturbances of the NSEF (black), we show a 1-minute time series of a 3 cm thick plastic scintillator of the STAND3 detector; the detector's threshold is ≈5 MeV. There is no enhancement of the count rate, i.e., no TGE observed. As the opposite, in Fig. 2(b), we see a sizeable enhancement in the count rate of the ORTEC spectrometer, i.e., the radon progeny was lifted in the atmosphere and caused additional gamma ray flux enhancing the NGR. The quantitative measure of these enhancements is shown in Table II.

Table II is similar to Table I, except all four selected events (with radon progeny radiation and without particle avalanches) were measured by the ORTEC spectrometer located within the lead cover. The average count rate with statistical errors is shown in the last row. Comparing Tables I and II, we can see that the hourly count rate of 511 keV gamma rays increased slightly from 2927 to 2973 counts per hour. However, the count of the 214Bi isotope increased by approximately 2.5 times from 557 to 1378 counts per hour. Despite this, the overall count rate only increased by 9% from 67990 to 74066 counts per hour, as shown in Fig. 2(a). Therefore, we can conclude that after introducing the lead filter, radon progeny gamma radiation does not contaminate the selected sample of the 511 keV annihilation gamma rays. This allows us to investigate the

TABLE II. One-hour count rates of NGR for four selected non-TGE events.

| Counts per hour | Sum MeV | 0.511 MeV | 214Pb 0.352 MeV | 214Bi 0.609 MeV | 214Bi 0.768 MeV | 228AC 0.911 MeV | 214Bi 1.12 MeV | 40K 1.46 MeV | 214Bi 1.76 MeV | 214Bi 2.2 MeV | 208Tl 2.61 MeV | Cosmic ray+ Compton scatter |
|---|---|---|---|---|---|---|---|---|---|---|---|---|
| Energy range | [0.3–3] | [0.47–0.552] | [0.324–0.38] | [0.56–0.66] | [0.7–0.83] | [0.84–0.98] | [1–1.2] | [1.34–1.57] | [1.62–1.89] | [2–2.4] | [2.41–2.82] | [0.3–3] |
| 2 June 15:50 16:50 | 73105 | 2958 | 1460 | 1274 | 551 | 598 | 657 | 1498 | 372 | 256 | 248 | 63233 |
| 3 June 15:32 16:32 | 72631 | 3039 | 1559 | 1281 | 524 | 618 | 646 | 1497 | 388 | 278 | 249 | 62552 |
| 4 June 18:07 19:07 | 72621 | 2938 | 1555 | 1471 | 502 | 435 | 631 | 1499 | 372 | 258 | 246 | 62714 |
| 09 June 17:10 18:10 | 77907 | 2956 | 1555 | 1485 | 552 | 594 | 706 | 1496 | 449 | 275 | 247 | 67592 |
| Mean count | 74066 ± 2571 | 2973 ± 45 | 1532 ± 48 | 1378 ± 116 | 532 ± 24 | 561 ± 85 | 660 ± 32 | 1498 ± 1 | 395 ± 37 | 267 ± 11 | 248 ± 1 | 64023 ± 2397 |

positron intensity's dependence (via its proxy 511 keV gamma ray flux) on the positive and negative disturbances of the NSEF by selecting relevant TGE events. Comparing Tables I and II, we also notice that the potassium-40 isotope is practically stable and is not affected by the NSEF.

## IV. BOOST OF THE POSITRON FLUX DURING TGEs AT POSITIVE AND NEGATIVE NSEFs

Figure 3 shows the storms from June 21–24, 2023, with 10 TGEs occurring (blue vertical lines in the count rate time series). The NSEF disturbances (black) and distance to

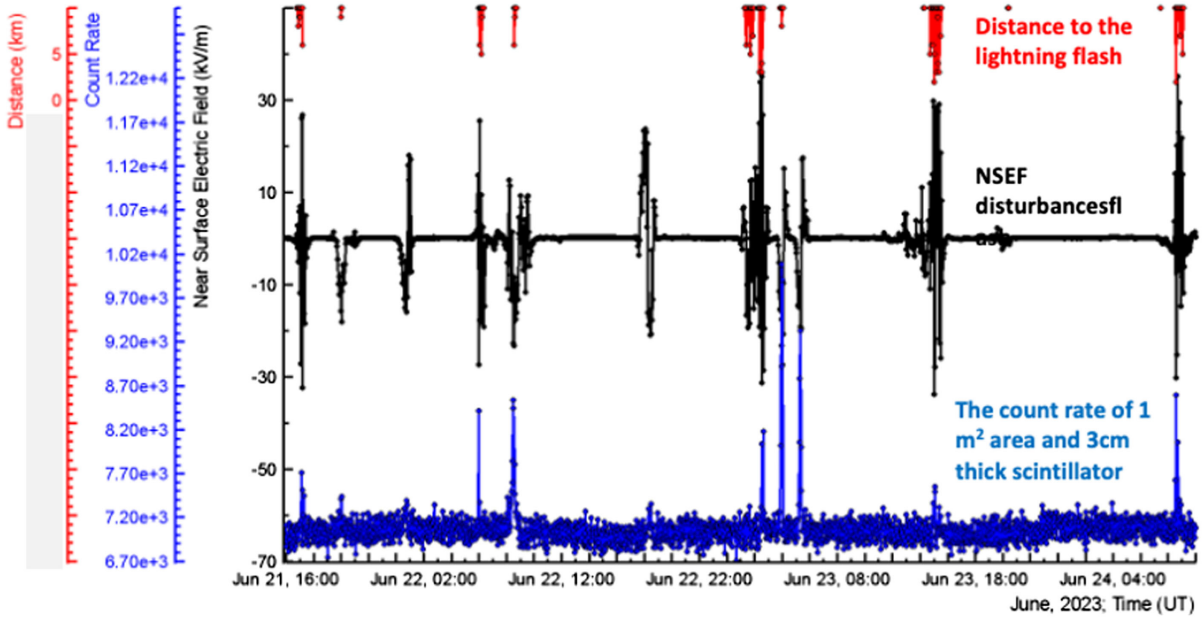


FIG. 3. Disturbances of the NSEF (black) and distances to lightning flashes (red) measured by BOLTEK's EFM 100 sensor; a 1-minute time series of the count rates measured by the 3 cm thick scintillator of the STAND3 detector's upper scintillator (blue, the energy threshold ≈5 MeV).

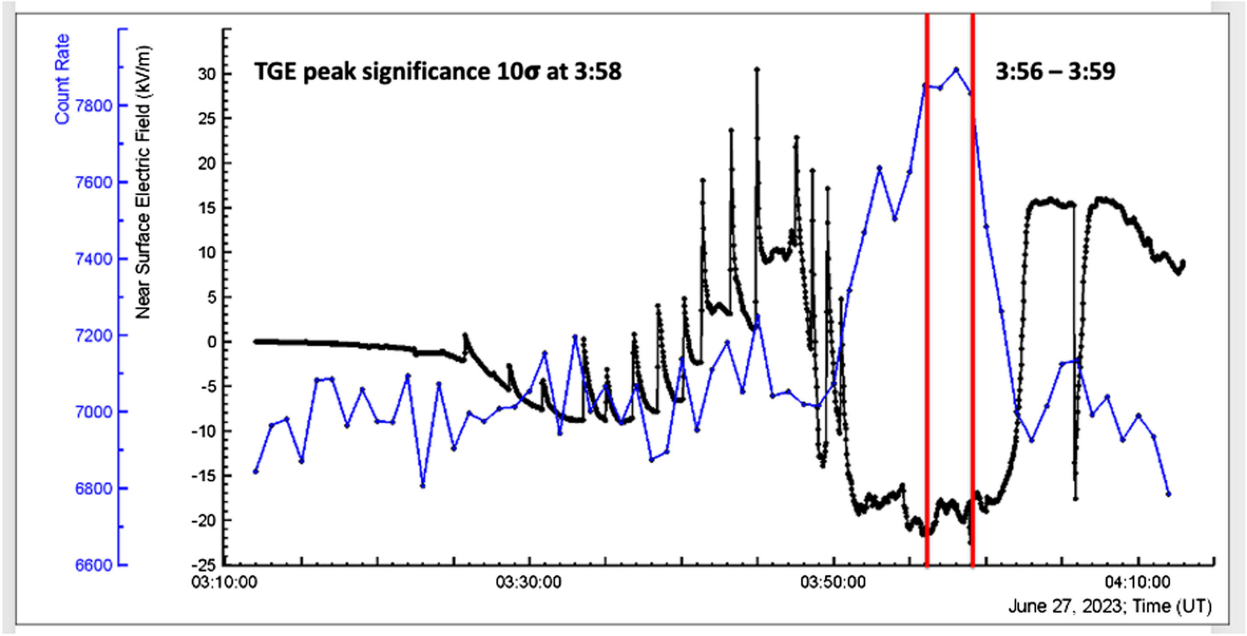


FIG. 4. Time series of 1-minute count rates of 3 cm thick plastic scintillator and 1 s time series of the disturbances of NSEF measured by EFM 100 sensor. The red lines outline 3 minutes of maximum TGE flux for which spectrograms were obtained with the ORTEC spectrometer.

TABLE III. One-minute count rates of main isotopes contributing to NGR for four selected TGE events at negative NSEF.

| Counts per minute | Sum 0.3–3 MeV | 0.511 MeV | 214Pb_ 0.352 MeV | 214Bi_ 0.609 MeV | 214Bi_ 0.768 MeV | AC_228 0.911 MeV | 214Bi_ 1.12 MeV | 40K 1.46 MeV | 214Bi_ 1.76 MeV | 214Bi_ 2.2 MeV | 208Tl_ 2.61 MeV | Cosmic rays+ Compton scatter |
|---|---|---|---|---|---|---|---|---|---|---|---|---|
| Energy range | [0.3–3] | [0.47–0.552] | [0.324–0.38] | [0.56–0.66] | [0.7–0.83] | [0.84–0.98] | [1–1.2] | [1.34–1.57] | [1.62–1.89] | [2–2.4] | [2.41–2.82] | [0.3–3] |
| 11 June 12:44–12:47 | 180 | 16 | 26 | 21 | 16 | 12 | 16 | 1 | 13 | 12 | 0 | 47 |
| % | 100,0 | 8,9 | 14,4 | 11,7 | å | 6,7 | 8,9 | 0,6 | 7,2 | 6,7 | 0,0 | 26,1 |
| 22 June 08:30–08:33 | 306 | 24 | 46 | 46 | 16 | 14 | 26 | 2 | 16 | 20 | 1 | 95 |
| % | 100,0 | 7,8 | 15,0 | 15,0 | 5,2 | 4,6 | 8,5 | 0,7 | 5,2 | 6,5 | 0,3 | 31,0 |
| 23 June 03:55–03:58 | 737 | 32 | 35 | 35 | 17 | 8 | 8 | 0 | 4 | 8 | 2 | 588 |
| % | 100,0 | 4,3 | 4,7 | 4,7 | 2,3 | 1,1 | 1,1 | 0,0 | 0,5 | 1,1 | 0,3 | 79,8 |
| 27 June 03:56–03:59 | 161 | 10 | 21 | 11 | 14 | 10 | 10 | 3 | 13 | 12 | 2 | 55 |
| % | 100,0 | 6,2 | 13,0 | 6,8 | 8,7 | 6,2 | 6,2 | 1,9 | 8,1 | 7,5 | 1,2 | 34,2 |
| Mean count | 346 ± 268 | 21 ± 10 | 32 ± 11 | 28 ± 15 | 16 ± 1 | 11 ± 3 | 15 ± 8 | 2 ± 1 | 12 ± 5 | 13 ± 5 | 1 ± 1 | 196 ± 162 |
| Mean % | | 6,8±1,7 | 11,8±4,8 | 9,6±4,7 | 6,3±3,1 | 4,6±2,5 | 6,2±3,6 | 0,8±0,7 | 5,3±3,4 | 5,4±2,9 | 0,5±0,4 | 42,8±24,9 |

lightning flash (red) are measured by the BOLTEK's EFM 100 electric mill and particle flux by the 3 cm thick 1 $m^2$ area plastic scintillator.

We select four TGE events that occurred during negative NSEF. The dipole between the main negative layer in the middle of the cloud and its mirror in the Earth accelerates electrons downward. We select TGEs with a significance larger than $10\sigma$. We assume the Gaussian distribution of the fair-weather cosmic ray flux and estimate sampling mean and variance before the TGE started. One of the four selected TGEs is shown in Fig. 4. The TGE prolongs 10 minutes, and lightning flashes do not terminate it. Multiple lightning flashes occurred before and after TGE. We select 3 minutes at the maximum particle flux and minimum NSEF (≈−20 kV/m). The ORTEC spectrograms normalized to 1 minute are shown in Table III.

In Table III, we show the intensity of each isotope and their percent relative to the total flux. In the last two rows, we summarize four TGE measurements by showing sampling mean and statistical error. The 511 keV line mean enhancement is 6.8 ± 1.7%. Radon chain isotope enhancement was even larger; however, as shown in the previous section, they do not significantly influence the 511 keV line. As expected, the 40 K and 208Tl isotope enhancement are within statistical errors because NSEF does not affect their atmospheric concentration. The enhancement of the 511 keV line is due to a significant enhancement of the TGE gamma ray flux. We select large TGE with peak significance 10–36$\sigma$. Thus, the number of TGE particles (mainly gamma rays) in the avalanches increased by 10–40%. Due to the pair production process, additional

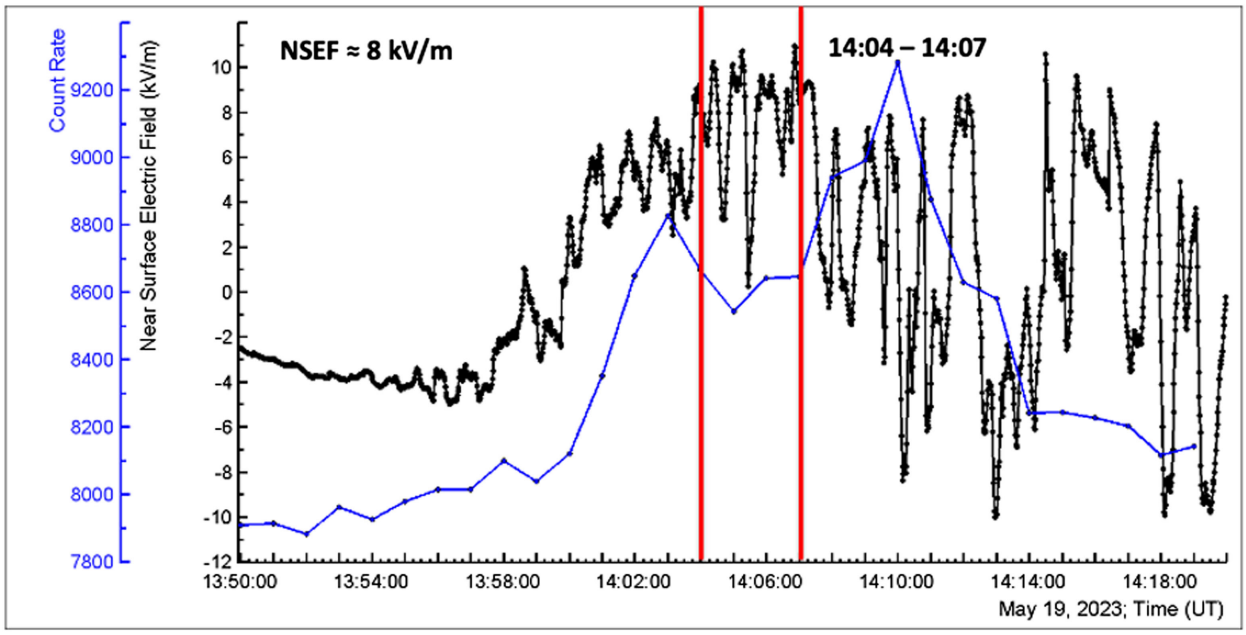


FIG. 5. Time series of 1-minute count rates of 3 cm thick plastic scintillator and 1 s time series of the disturbances of NSEF measured by EFM 100 sensor. By the read lines, we outline 3 minutes of maximum NSEF, which spectrograms were obtained with the ORTEC spectrometer.

TABLE IV. One-minute count rates of main isotopes contributing to NGR for four selected TGE events at positive NSEF.

| Counts per minute | Sum 0.3–3 MeV | 0.511 MeV | 214Pb_ 0.352 MeV | 214Bi_ 0.609 MeV | 214Bi_ 0.768 MeV | AC_ 228 0.911 MeV | 214Bi_ 1.12 MeV | 40K_ 1.46 MeV | 214Bi_ 1.76 MeV | 214Bi_ 2.2 MeV | 208Tl_ 2.61 MeV | Cosmic rays+ Compton scatter |
|---|---|---|---|---|---|---|---|---|---|---|---|---|
| Energy range | [0.3–3] | [0.47–0.552] | [0.324–0.38] | [0.56–0.66] | [0.7–0.83] | [0.84–0.98] | [1–1.2] | [1.34–1.57] | [1.62–1.89] | [2–2.4] | [2.41–2.82] | [0.3–3] |
| 19 May 14:04–14:07 | 166 | 18 | 11 | 16 | 15 | 12 | 13 | 1 | 13 | 10 | 1 | 56 |
| % | 100,0 | 11 | 6,6 | 9,6 | 9,0 | 7,2 | 7,8 | 0,6 | 7,8 | 6,0 | 0,6 | 33,7 |
| 31 May 08:36–08:39 | 194 | 19 | 26 | 21 | 20 | 14 | 13 | 2 | 15 | 11 | 2 | 51 |
| % | 100,0 | 10 | 13,4 | 10,8 | 10,3 | 7,2 | 6,7 | 1,0 | 7,7 | 5,7 | 1,0 | 26,3 |
| 21 June. 17:12–17:15 | 292 | 31 | 42 | 43 | 29 | 15 | 25 | 2 | 16 | 14 | 2 | 73 |
| % | 100,0 | 11 | 14,4 | 14,7 | 9,9 | 5,1 | 8,6 | 0,7 | 5,5 | 4,8 | 0,7 | 25,0 |
| 24 June 08:43–08:46 | 214 | 23 | 29 | 34 | 25 | 14 | 15 | 2 | 12 | 13 | 1 | 46 |
| % | 100,0 | 11 | 13,6 | 15,9 | 11,7 | 6,5 | 7,0 | 0,9 | 5,6 | 6,1 | 0,5 | 21,5 |
| mean Coun | $217 \pm 54$ | $23 \pm 6$ | $27 \pm 13$ | $29 \pm 12$ | $22 \pm 6$ | $14 \pm 1$ | $17 \pm 1$ | $2 \pm 1$ | $14 \pm 2$ | $12 \pm 2$ | $2 \pm 1$ | $57 \pm 12$ |
| mean % | | 10,8±0,2 | 12,0±3,6 | 12,8±3,0 | 10,2±1,1 | 6,5±1,0 | 7,5±0,8 | 0,8±0,2 | 6,7±1,3 | 5,6±0,6 | 0,7±0,2 | 26,6±5,2 |

TABLE V. Comparison of enhancements of radionuclides and 511 keV line at negative and positive NSEF.

| Counts per minute per $m^2$ | 0.511 MeV | 214Pb 0.352 MeV | 214Bi 0.609 MeV | Sum of radionuclides | Cosmic rays+ Compton scatter |
|---|---|---|---|---|---|
| Energy range MeV | [0.47–0.552] | [0.324–0.38] | [0.56–0.66] | [0.7–3] | [0.3–3] |
| TGE at negative NSEF | $3534 \pm 1651$ | $5517 \pm 1894$ | $4871 \pm 2654$ | $11897 \pm 3428$ | $33836 \pm 27931$ |
| [%] | $6,8 \pm 1,7$ | $11,8 \pm 4,8$ | $9,6 \pm 4,7$ | $29,0 \pm 15,6$ | $42,8 \pm 24,9$ |
| TGE at positive NSEF | $3922 \pm 1019$ | $4655 \pm 2194$ | $4914 \pm 2119$ | $14095 \pm 2735$ | $9741 \pm 2023$ |
| [%] | $10,8 \pm 0,2$ | $12,0 \pm 3,6$ | $12,8 \pm 3,0$ | $37,8 \pm 2,0$ | $26,6 \pm 5,2$ |

gamma rays enhance the number of positrons and, respectively, the number of "annihilations" 511 keV gamma rays.

Selecting TGE events occurring during positive NSEF, we choose the minutes of the largest NSEF; see Fig. 5 (note that the selected time does not coincide with TGE maximum flux at 14:10). The positive NSEF is an indicator of the LPCR maturity and consequently, the emergence of the third dipole in the lower atmosphere. The electric field between LPCR and its mirror in the Earth accelerates positrons downward, enhancing the number of 511 keV gamma rays that reach the spectrometer. The mean enhancement of the 511 keV gamma rays reaches $10.8 \pm 0.2\%$, significantly more than $6.8 \pm 1.7$ at the negative field, see Table IV. Thus, by comparing Tables III and IV, we can estimate the 511 keV gamma rays' enhancement due to positron acceleration at approximately 4%. In the last column of Tables III and IV, we show the share in the NGR of cosmic rays, i.e., TGE particles and Compton scattered gamma rays from the radionuclides decay. For TGEs selected at negative NSEF, the share is larger than one selected at positive flux due to larger TGEs occurring at the negative field compared to the positive field's TGEs. During large TGEs, the percentage of TGE particles in the NGR can reach 90% or more, like at exceptional TGE that occurred at Aragats on 23 May 2023.

## V. CONCLUSION

In our previous measurements, we demonstrate that the atmospheric electric field during thunderstorms modulates fluxes of cosmic ray electrons and gamma rays [12], muons [13], and neutrons [14]. This research shows that positron flux is also modulated by the emerged charged structures in the thundercloud. As shown in Table V (count rates were recalculated to 1 $m^2$), we measure significant enhancement of the 511 keV gamma ray flux during TGEs occurred at positive NSEF (≈400 gamma rays per minute per $m^2$). The enhanced 511 KeV flux indicates positron acceleration in the dipole between the cloud base and the ground. A RREA is developing above the dipole between the main negative layer and LPCR. Thus, by the 511 keV gamma ray flux measurements, we can confirm the scenario of the LPCR emergence and its role in cosmic ray flux modulation.

The data for this study is available by the multivariate visualization software platform ADEI on the WEB page of the Cosmic Ray Division (CRD) of the Yerevan Physics Institute [14].

## ACKNOWLEDGMENTS

We thank the staff of the Aragats Space Environmental Center for safeguarding the operation of experimental facilities on Aragats. The authors acknowledge the support of the Science Committee of the Republic of Armenia (Research Project No. 21AG-1C012) in the modernization of the technical infrastructure of high-altitude stations.

[1] J. Küttener, The electrical, and meteorological conditions inside thunderclouds, J. Meteorol. **7**, 322 (1950).
[2] C. T. R. Wilson, The acceleration of betta-particles in strong electric fields such as those of thunder-clouds, Proc. Cambridge Philos. Soc. **22**, 534 (1924).
[3] A. V. Gurevich, G. Milikh, and R. Roussel-Dupre, Runaway electron mechanism of air breakdown and preconditioning during a thunderstorm, Phys. Lett. A **165**, 463 (1992).
[4] A. Chilingarian, A. Daryan, K. Arakelyan, A. Hovhannisyan, B. Mailyan, L. Melkumyan, G. Hovsepyan, S. Chilingaryan, A. Reymers, and L. Vanyan, Ground-based observations of thunderstorm-correlated fluxes of high-energy electrons, gamma rays, and neutrons, Phys. Rev. D **82**, 043009 (2010).
[5] A. Chilingarian, G. Hovsepyan, and A. Hovhannisyan, Particle bursts from thunderclouds: Natural particle accelerators above our heads, Phys. Rev. D **83**, 062001 (2011).
[6] R. Feynman, R. B. Leighton, and M. Sands, The Feynman lectures on physics in *Electricity in the Atmosphere*, edited by M. A. Gottlieb and R. Pfeiffer (California Institute of Technology, New York, 1963), Vol. II, Chap. 9.
[7] E. Williams, The tripole structure of thunderstorms, J. Geophys. Res. **94**, 13151 (1989).
[8] A. Nag and V. Rakov, Some inferences on the role of lower positive charge region in facilitating different types of lightning, Geophys. Res. Lett. **36**, L05815 (2009).
[9] A. Chilingarian, S. Chilingaryan, T. Karapetyan, L. Kozliner, Y. Khanikyants, G. Hovsepyan, D. Pokhsraryan, and S. Soghomonyan, On the initiation of lightning in thunderclouds, Sci. Rep. **7**, 1371 (2017).
[10] A. Chilingarian, G. Hovsepyan, A. Elbekian, T. Karapetyan, L. Kozliner, H. Martoian, and B. Sargsyan, Origin of enhanced gamma radiation in thunderclouds, Phys. Rev. Res. **1**, 033167 (2019).
[11] A. Chilinarian, G. Hovsepyan, and B. Sargsyan, Circulation of Radon progeny in the terrestrial atmosphere during thunderstorms, Geophys. Res. Lett. **47**, e2020GL091155 (2020).
[12] A. Chilingarian, G. Hovsepyan, and M. Zazyan, Muon tomography of charged structures in the atmospheric electric field, Geophys. Res. Lett. **48**, e2021GL094594 (2021).
[13] A. Chilingarian, N. Bostanjyan, and L. Vanyan, Neutron bursts associated with thunderstorms, Phys. Rev. D **85**, 085017 (2012).
[14] S. Chilingaryan, A. Chilingarian, V. Danielyan, and W. Eppler, The Aragats data acquisition system for highly distributed particle detecting networks, J. Phys. Conf. Ser. **119**, 082001 (2008).